ELSEVIER

NeuroImage

www.elsevier.com/locate/ynimg
NeuroImage 41 (2008) 801–812

Functional changes of apparent diffusion coefficient during visual stimulation investigated by diffusion-weighted gradient-echo fMRI

Tao Jin[a,*] and Seong-Gi Kim[a,b]

[a]*Department of Radiology, University of Pittsburgh, Pittsburgh, PA 15203, USA*
[b]*Department of Neurobiology, University of Pittsburgh, Pittsburgh, PA 15203, USA*

Received 14 December 2007; revised 14 February 2008; accepted 10 March 2008
Available online 20 March 2008

The signal source of apparent diffusion coefficient (ADC) changes induced by neural activity is not fully understood. To examine this issue, ADC-fMRI in response to a visual stimulus was obtained in isoflurane-anesthetized cats at 9.4 T. A gradient-echo technique was used for minimizing the coupling between diffusion and background field gradients, which was experimentally confirmed. In the small *b*-value domain ($b=5$ and 200 s/mm^2), a functional ADC increase was detected at the middle of the visual cortex and at the cortical surface, which was caused mainly by an increase in cerebral blood volume (CBV) and inflow. With higher *b*-values ($b=200$ and 1000–1200 s/mm^2), a functional ADC decrease was observed in the parenchyma and also at the cortical surface. Within the parenchyma, the ADC decrease responded faster than the BOLD signal, but was not well localized to the middle of visual cortex and almost disappeared when the intravascular signal was removed with a susceptibility contrast agent, suggesting that the decrease in ADC without contrast agent was mostly of vascular origin. At the cortical surface, an average ADC decrease of 0.5% remained after injection of the contrast agent, which may have arisen from a functional reduction of the partial volume of cerebrospinal fluid. Overall, a functional ADC change of tissue origin could not be detected under our experimental conditions.

Keywords: fMRI; BOLD; CBV; ADC; Neural activity; Cell swelling; Visual stimulation

Introduction

The apparent diffusion coefficient (ADC) is a measure of water mobility in an imaging voxel and has been widely applied in magnetic resonance imaging (MRI) to probe the structural and pathological information of brains *in vivo*. The ADC is obtained by two or more measurements that have different diffusion-weighting gradients (usually quantified by the *b*-value). Recently, activation-induced changes of ADC values have been observed and proposed to improve the spatial specificity of fMRI maps with respect to the conventional blood oxygenation level-dependent (BOLD) technique (Gangstead and Song, 2002; Jin et al., 2006c; Le Bihan et al., 2006; Song et al., 2003, 2002b; Zhong et al., 1998). However, because an imaging voxel often contains different water compartments with drastically different mobilities, the source of these ADC changes can be very complex. A functional change in the ADC can be induced by changes in blood volume and flow, and water diffusion characteristics in tissues. Furthermore, ADC measurement is dependent on many factors, such as the choice of *b*-values, the pulse sequence and form of diffusion gradients, experimental parameters (echo time and diffusion time, etc), and the partial volume effect. Therefore, careful examination of the signal source of observed functional ADC signals is crucial.

Functional ADC increases are generally observed in the small diffusion-weighting domain (usually $b\leq 200$ s/mm^2) due to the following three mechanisms: i) activity-induced increases in arterial blood volume and flow can increase ADC (Gangstead and Song, 2002; Jin et al., 2006c; Song et al., 2003, 2002b); ii) because ADC can be considered a weighted function of tissue and blood compartments, an increase in intravascular venous blood signals due to the BOLD effect will enhance weighting of the fast-flowing (venous) blood compartment, thus contributing to an elevation in the ADC (Jin et al., 2006c); and iii) for a pulsed-gradient spin-echo (PGSE) sequence, there can be significant coupling between the applied diffusion-weighting gradients and the extravascular susceptibility gradients (Hong and Dixon, 1992; Zhong et al., 1991). Hence, a functional decrease in blood susceptibility can lead to an ADC increase in the tissue compartment (Zhong et al., 1998); this effect persists in the large *b*-value domains due to its extravascular origin. In our previous PGSE experiments at 9.4 T, an ADC increase was observed in the small diffusion-weighting domain (with $b=2$ and 200 s/mm^2) (Jin et al., 2006c). The ADC increases mostly at the cortical surface area at short echo times (TE=16 ms) due to large

* Corresponding author. 3025 East Carson Street, University of Pittsburgh, Pittsburgh, PA 15203, USA. Fax: +1 412 383 6799.
E-mail address: taj6@pitt.edu (T. Jin).
Available online on ScienceDirect (www.sciencedirect.com).

1053-8119/$ - see front matter © 2008 Elsevier Inc. All rights reserved.
doi:10.1016/j.neuroimage.2008.03.014

intravascular BOLD signal changes. When the venous signal was minimized with relatively long TE values (≥28 ms) compared with T_2 of the venous blood, ADC-fMRI was found to be better localized to the middle cortical layer than spin-echo (SE) BOLD fMRI. However, the temporal resolution of SE-based ADC-fMRI was poor; thus, the temporal characteristics of the functional ADC increase could not be examined.

With moderate to high diffusion-weighting ($b \geq 200$ s/mm^2), transient ADC decreases have been reported in the human visual cortex (Darquie et al., 2001), which presumably originated from the tissue compartment because blood signals are greatly reduced due to the intravoxel incoherent motion (IVIM) effect (Le Bihan et al., 1986). Recently, a change in the diffusion-weighted (DW) fMRI signal with high *b*-values was found to be significantly faster (~2.4 s) than the BOLD response, and may reflect a transition of water from a fast diffusion pool to a slow diffusion pool during expansion of the neuronal cell membrane (Le Bihan et al., 2006). This mechanism, if confirmed, can potentially offer a more direct and more accurate mapping of brain activation than conventional hemodynamic-based contrasts, and would have great impact in the fMRI and neuroscience communities. However, due to the limited spatial resolution in human studies and the uncertainty of contributions from vascular and susceptibility effects, the exact signal source of these ADC and DW signal changes is controversial and requires further investigation (Kershaw et al., 2007; Miller et al., 2007). In our PGSE studies with $b=200$ and 800 s/mm^2 (Jin et al., 2006c), stimulation-induced ADC changes could not be observed in the brain parenchyma (Jin et al., 2006c). Note that in PGSE-ADC studies, the change in blood susceptibility may have counteracted and reduced the sensitivity of any weak ADC-decreasing effects within the parenchyma due to the aforementioned coupling between the diffusion-weighting gradient and the background field inhomogeneity. Therefore, it is necessary to re-examine ADC responses using pulse sequences that minimize such coupling effects.

In this report, the coupling effects between background and diffusion gradients were initially examined *in vivo* for gradient-echo (GE) and PGSE-ADC measurements after the blood susceptibility effect was systematically modulated by intravascular injections of a susceptibility contrast agent, monocrystalline iron oxide nanoparticle (MION). To reduce the coupling effect and obtain a higher temporal resolution, the GE sequence with bipolar diffusion-sensitizing gradients was employed for functional ADC studies of the visual cortex in isoflurane-anesthetized cat at 9.4 T. The specific goals were to investigate the spatial specificity and temporal characteristics of functional ADC responses and to determine the signal source of functional ADC decreases at high diffusion-weightings. To this end, cross-sectional images of the cortex were obtained, because the middle cortical layer (layer 4) is known to have the highest neural activity, cytochrome oxidase activity, and metabolic rate (McCasland and Woolsey, 1988; Tootell et al., 1988; Woolsey et al., 1996). If the ADC contrast indeed originates from neuronal cells, the highest ADC changes should occur in the middle of the cortex. To further ensure that the measured ADC response is not of intravascular origin, fMRI ADC studies were also performed using an injection of a small dose of MION. To explain our experimental observations, computer simulations were performed with a simple two-compartment (tissue and blood) model in Appendix A. Preliminary accounts of this work have been presented at scientific meetings (Jin and Kim, 2007; Jin et al., 2005).

Materials and methods

Animal preparation and stimulation

All animal protocols were approved by the Institutional Animal Care and Use Committee at the University of Pittsburgh. We performed rat studies for examining the effects of susceptibility gradients on GE versus PGSE-ADC measurements, and cat studies for investigating the source and spatial specificity of functional ADC changes.

Five Sprague–Dawley rats were anesthetized with 5% isoflurane in a mixture of medical air and O_2 gases, and intubated for ventilation. Once the animals were fully anesthetized, the isoflurane level was reduced to 2.0% with a 7:3 medical air/O_2 mixture for surgery. During the MR experiments, the isoflurane level was maintained at about 1.5%. The femoral artery and vein were catheterized for blood pressure monitoring, and fluid administration and injection of MION, respectively.

Fourteen female adolescent cats weighing 0.8–1.7 kg were used in a total of 16 functional ADC studies (two animals were used twice). The detailed animal preparation procedure has been described previously (Jin et al., 2006b; Zhao et al., 2004). Briefly, cats were anesthetized under 0.8−1.3% isoflurane and artificially ventilated with a 7:3 medical air/O_2 mixture. End-tidal CO_2 level was kept within 3.5±0.5%, and the rectal temperature was controlled at 38.5±0.5 °C using a water-circulating pad. The cephalic or femoral vein was cannulated to deliver pancuronium bromide (~0.2 mg/kg/h) and maintenance fluid. For visual stimulation, binocular, full-field, black and white, and square-wave drifting gratings (spatial frequency 0.15 cycle/degree and temporal frequency 2 cycles/s) were used. Stationary gratings of the same spatial frequency were presented as control.

MR experiments

All MR experiments were carried out on a 9.4 T/31-cm horizontal magnet (Magnex, UK) interfaced with a Unity INOVA console (Varian, Palo Alto, CA). The actively shielded gradient coil has an inner diameter of 12 cm, strength of 40 G/cm, and a rise time of 130 μs (Magnex, Abington, UK). A 1.6-cm diameter surface coil was placed on top of the animal's head and used for radiofrequency (RF) excitation and reception. Fast low-angle shot (FLASH) images were obtained to identify the anatomical structures in the brain and to place the region of interest (ROI) close to the isocenter of the magnetic field. Magnetic field homogeneity was optimized by localized shimming over a $\sim 10 \times 5 \times 5$ mm^3 brain volume to yield a water spectral linewidth of 16–25 Hz. For fMRI studies, multi-slice "scout" GE echo planar imaging (EPI) BOLD studies were performed in the cat visual cortex, then a single 2-mm coronal plane was chosen that was nearly perpendicular to the cortical surface and gave a high-quality echo planar image as well as a robust BOLD contrast. All experiments were conducted on that slice with a 2×2 cm^2 field of view and a 64×64 matrix size. For T_1-weighted anatomical reference, an inversion recovery image was acquired by a four-shot SE-EPI with a 128×128 matrix.

Three experiments were performed: i) PGSE vs. GE-ADC measurements without any stimulation, ii) functional GE-ADC studies without MION, and iii) functional GE-ADC studies after injection of MION. The strength of the diffusion-weighting, *b*-value, is described as $(\gamma\, \delta\, g)^2 \cdot (\Delta - \delta/3)$, where γ is the gyromagnetic ratio, g is the strength of applied diffusion gradients, δ is the duration of one lobe of the gradient pulse, and Δ is the time interval between the two lobes of the diffusion gradients. The diffusion time t_d is $(\Delta - \delta/3)$. To

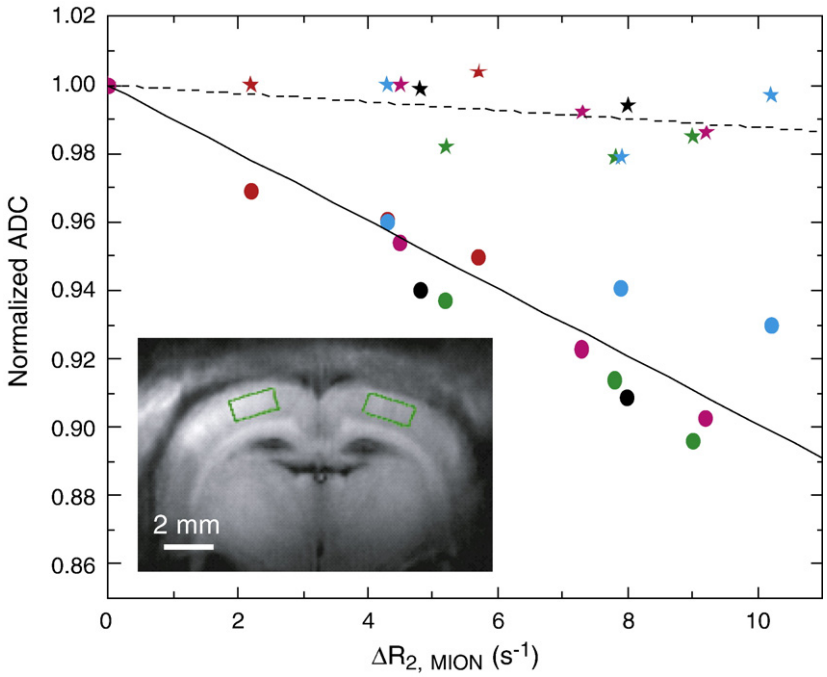

Fig. 1. Normalized ADC values measured by diffusion-weighted GE-EPI (stars) and PGSE-EPI (circles) sequences as a function of susceptibility change ($\Delta R_{2,\ MION}$) caused by various doses of MION injection. ADC values were obtained from rat cortical areas, shown as green ROIs in an anatomic image (Inset). A total of 19 measurements for both GE and PGSE were performed on 5 rats, represented by different colors. Before the injection of MION, the baseline ADC value was 0.69 ± 0.02 and $0.73\pm0.01\times10^{-3}$ mm^2/s ($n=5$) for GE and PGSE measurements, respectively. Dashed and solid lines indicate linear regressions of GE and PGSE data.

shorten δ and consequently TE, the diffusion gradients were applied on all three axes, and the b-values were modulated by varying the strength of the diffusion gradients. For fMRI studies (Experiments #2 and #3), two or three b-values were cycled in each run. The order of the two b-values was alternated for different fMRI runs, while the order of the three b-values was fixed in one animal, but varied for different animals.

Experiment #1

To evaluate the effect of the susceptibility gradient on extravascular ADC measurements, rat experiments ($n=5$) were performed with injection of various doses (0 to 15 mg/kg) of MION. Each animal was measured before and after two or three injections; a total of 19 data points were obtained from 5 animals for both GE and PGSE measurements. Four b-values of 200, 600, 1000, and 1500 s/mm^2 were used, in which the blood signal is likely to be crushed. For GE-EPI ADC studies, the experimental parameters were $\delta=4.5$ ms, $\Delta=9$ ms, TE=21 ms, and TR=1 s. For PGSE-EPI, a double spin-echo sequence was used in which two unipolar diffusion gradients were placed on both sides of the second 180° refocusing pulse (Jin et al., 2006b); the imaging parameters were $\delta=3.9$ ms, $\Delta=20.3$ ms, TE=45 ms, and TR=2 s. The blood susceptibility effect was indirectly quantified by measuring the change of R_2 ($=1/T_2$) induced by each MION injection using SE-EPI with five TE values of 25, 30, 35, 40, and 45 ms.

Experiment #2

ADC-fMRI values without MION were obtained by single-shot GE-EPI with $\delta=3.9$ ms, $\Delta=6.3$ ms ($t_d=5$ ms), TE=18 ms, and TR=0.5 s or 1.0 s. A shifted-echo scheme was adopted to reduce the effective TE, wherein the zero k-space line was shifted by 24 k-space lines from the center of data acquisition and located at the eighth line of the k-space trajectory (Fig. 1C in (Windischberger and Moser, 2000)). Six studies were performed with a TR of 0.5 s; three b-values of 5, 200, and 1000 s/mm^2; and an RF power (B_1) optimized for the signal-to-noise ratio (SNR) at the primary visual cortex (an effective Ernst angle over the cortex). To examine the contribution of inflow effects to functional ADC changes, three additional studies were performed with a TR of 1.0 s, two b-values of 200 and 1200 s/mm^2, and half of B_1 relative to the former (TR of 0.5 s studies). The effective temporal resolution was 1.5 s for the former and 2.0 s for the latter (TR of 1 s studies). The stimulation paradigm included 30 s of control, 30 s stimulation, and 30–40 s control. The former was averaged for 50–70 runs, and the latter ~80 runs to roughly match the baseline SNR of ADC images between the two different TR experiments.

Experiment #3

A 5 mg Fe/kg dose of MION was injected to fully remove the intravascular signals ($n=7$). The half-life of MION particles in blood was measured to be 4–5 h. In each fMRI run, two b-values of 50 and 1050 s/mm^2 were cycled, and images were acquired using two-segmented GE-EPI with center-out k-space sampling and navigator echo correction (Kim et al., 1996). Imaging parameters were $\delta=4.2$ ms, $\Delta=6.4$ ms ($t_d=5$ ms), TE=16 ms, TR=0.5 s/segment and 1.0 s/image, and effective TR=2 s. The stimulation paradigm included 30 s control (15 images for each b-value), 30 s stimulation, and 40 s control images, and 50–70 runs were averaged.

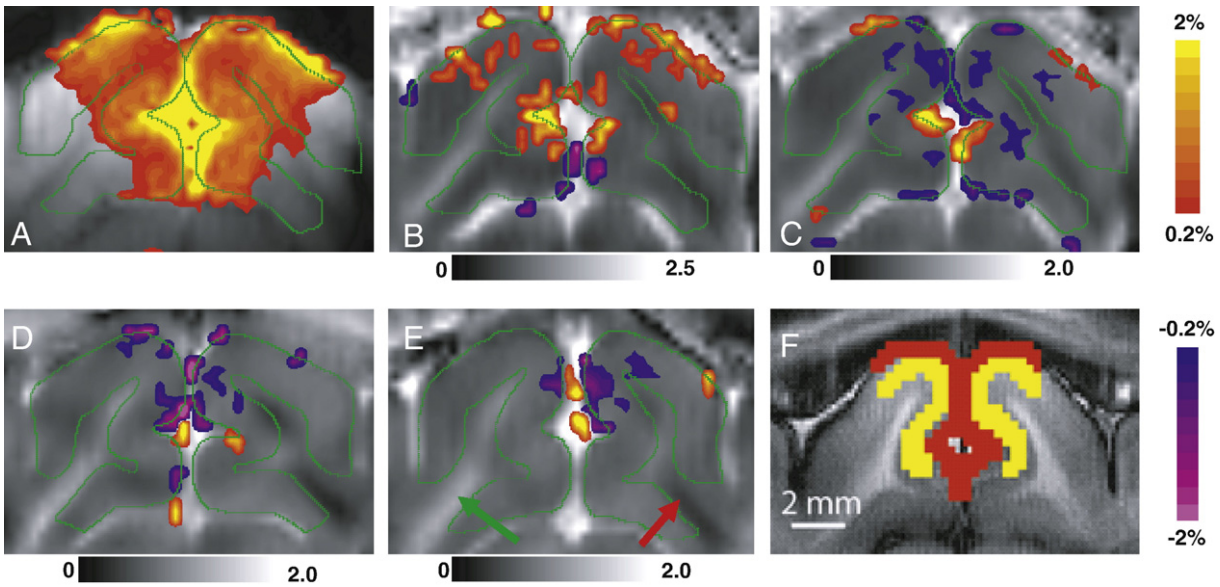

Fig. 2. Functional studies without MION. BOLD (A) and ADC percentage change maps obtained from the small *b*-value pair with $b=5$ and 200 s/mm^2 (B) and the large *b*-value pair with $b=200$ and 1000 s/mm^2 (C), overlaid on corresponding baseline images for one representative animal. The BOLD map was obtained from data with $b=5$ s/mm^2. The gray matter areas were outlined by green contours. Baseline ADC values are indicated by the horizontal grayscale bars in units of 10^{-3} mm^2/s. The diffusion anisotropy due to different orientations of white matter can be seen as light gray (green arrow) and dark (red arrow) pixels in (E). Note that the diffusion-weighted images and the calculated ADC images co-registered well with the anatomical image. For the small *b*-value pair, positive ADC changes were observed due to hemodynamic responses. ADC values obtained from the large *b*-value pair decreased at the parenchyma, while they decreased and increased at different locations of the cortical surface. To examine whether the inflow effect contributed to ADC changes, the inflow effect was reduced using a lower flip angle and a longer TR; ADC maps from the large *b*-value pair are shown for two other animals (D and E). Clearly, the number of active pixels is reduced, suggesting that ADC change is likely to be due to hemodynamic responses. For further quantitative analysis, cortical surface (red) and middle cortical ROIs (yellow) were selected from a T_1-weighted SE-EPI image (F).

Data analysis

Data were analyzed with in-house Matlab® programs and STIMULATE software (Strupp, 1996). Two types of quantitative analyses were performed; functional maps were generated from pixel-by-pixel analysis, and regional analyses were performed on the region of interest. Statistical analyses were performed using paired or unpaired *t*-tests (Origin 7.0, Northampton, MA, USA). Data are reported as mean±standard deviation (SD) unless noted otherwise.

Experiment #1

In rat studies, before and after each MION injection, R_2 and ADC maps were calculated from five TE-value and four *b*-value data, assuming a single exponential decay of TE and *b*-value, respectively. Then, a change in R_2 induced by MION ($\Delta R_{2,\mathrm{MION}}$) for cortical ROIs (see Fig. 1 inset) was calculated by the difference between R_2 values without and with MION, and plotted against ADC values normalized by ADC before MION injection.

Experiment #2 and #3

All fMRI runs with the same diffusion-weightings were averaged. For experiments with two *b*-values, images with the same *b*-value acquired in runs with two *b*-value orders were combined at each data point to obtain time-matched *b*-value runs. Then, one series of ADC images was calculated from pixel-wise mono-exponential fittings of two *b*-value images at each time point. For fMRI experiments with sequential sampling of three *b*-values, data with different *b*-values were obtained at different time points, and thus were temporally interpolated to match the time origins. Two time series of ADC images were calculated from pixel-wise mono-exponential fittings of signal intensities on two *b*-values: one from images with $b=5$ and 200 s/mm^2 (also referred as to a small *b*-value pair) and the other from images with $b=200$ and 1000 s/mm^2 (also referred as to a large *b*-value pair). Overall, three- and two-*b*-value runs were reprocessed to five and three datasets, respectively; three *b*-value data resulted in three DW-fMRI and two ADC-fMRI runs, while two *b*-value data produced two DW-fMRI and one ADC-fMRI run.

Student's *t*-test was performed on a pixel-by-pixel basis to compare 30-s pre-stimulus data versus data acquired at 6 s to 30 s after onset of stimulation. First, a p-value<0.05 (uncorrected for multiple comparisons) was chosen, and a minimal cluster size of three contiguous pixels was applied. Then, the percentage signal change was calculated for the activated pixels. DW-fMRI with *b*-value of 5 s/mm^2 before MION injection is considered BOLD fMRI. In order to determine the locations of active pixels in ADC-fMRI maps, a scatter plot of ADC change versus baseline ADC values was obtained.

To compare time courses of functional responses, two ROIs were hand-traced at ~2-pixel thickness to encompass approximately the middle and surface one-third of the cortex based on the anatomic image, regardless of whether these pixels passed the statistical threshold. The middle cortical ROI contains mostly tissue and small vessels, while the cortical surface ROI contains tissue, large surface vessels, and a significant partial volume of CSF. At the middle cortical ROI, the temporal SNR and contrast-to-noise ratio (CNR)

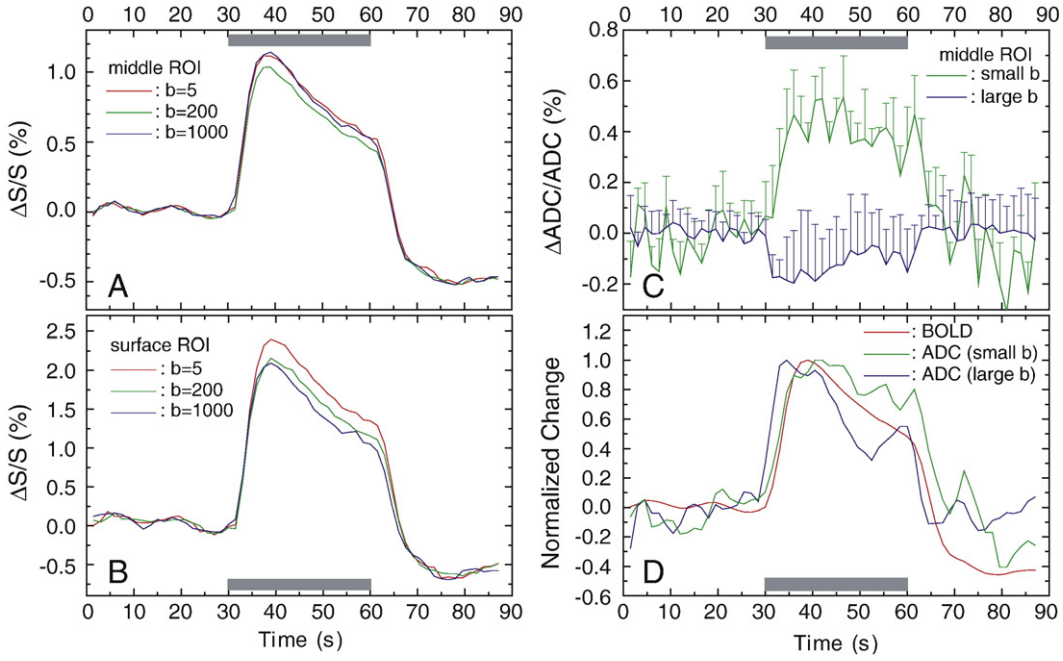

Fig. 3. Average time courses ($n=6$) of fMRI data without MION. Three DW-fMRI time courses were obtained from the middle cortical ROI (A) and surface ROI (B). The average ADC time course from the middle cortical ROI (C) showed an increase in ADC for the small *b*-value pair, but a decrease for the large *b*-value pair. To compare dynamic properties, BOLD (from $b=5$ s/mm^2) and ADC time courses at the middle cortical ROI (D) were normalized by its corresponding peak and smoothed by a three-point temporal average. Gray bars: stimulation period; error bars: standard errors of means.

were calculated; the former was from the averaged pre-stimulus baseline signal divided by the temporal SD of the pre-stimulus baseline images, and the latter was signal difference (ΔS) between the baseline and activation period divided by the baseline temporal SD.

Results

Gradient-echo vs. pulsed-gradient spin-echo ADC measurements

Due to the coupling between diffusion-weighting and background field gradients, extravascular water ADC values can be sensitive to the susceptibility effect induced by paramagnetic deoxyhemoglobin. Consequently, tissue ADC values can be influenced by BOLD signals. To examine this effect, GE-EPI with bipolar diffusion gradients and PGSE-EPI with unipolar gradients were measured in rat brain at various doses of MION. Fig. 1 shows the normalized ADC values versus $\Delta R_{2,\mathrm{MION}}$, obtained from cortical ROIs (inset image). Before the injection of MION, the baseline ADC value was 0.69 ± 0.02 and $0.73\pm0.01\times10^{-3}$ mm^2/s ($n=5$) for GE and PGSE measurements, respectively. $\Delta R_{2,\mathrm{MION}}$ reflects the magnitude of elevated field inhomogeneity due to the addition of MION. For PGSE-EPI, the measured ADC decrease was almost linearly dependent on $\Delta R_{2,\mathrm{MION}}$, and can be fitted as: normalized ADC$=1-0.01\cdot\Delta R_{2,\mathrm{MION}}$ ($R=0.90$), where $\Delta R_{2,\mathrm{MION}}$ is expressed in units of s^{-1}. For GE-EPI, the dependence on $\Delta R_{2,\mathrm{MION}}$ was much weaker, and a linear regression fit gave: normalized ADC$=1-0.0012\cdot\Delta R_{2,\mathrm{MION}}$ ($R=0.55$). When the administration of 5 mg/kg MION induced $\Delta R_{2,\mathrm{MION}}$ of about 5 s^{-1} in the parenchyma, the decrease in the ADC induced by susceptibility effects was 5% and 0.6% in PGSE and GE measurements, respectively. Our results indicate that the GE-EPI sequence with bipolar gradients is insensitive to field inhomogeneity. Hence, the GE technique with bipolar gradients was used for all functional ADC studies.

GE-ADC-fMRI: Spatial specificity and dynamics

GE fMRI with three *b*-values was performed on cat visual cortex. Fig. 2A–C show the results from one representative animal. Baseline ADC images (Fig. 2B and C) show that the ADC value of gray matter (outlined by green contours) is much lower than that at the surface of the cortex and between the two hemispheres, where CSF exists (bright pixels). The diffusion anisotropy for different white matter orientations can be seen as light gray and dark pixels in the baseline ADC image (green and red arrows in Fig. 2E). In GE BOLD ($b=5$ s/mm^2, Fig. 2A), the highest positive BOLD signal change (yellow pixels) appeared at the cortical surface and between the two hemispheres. The functional ADC map that was obtained from the small *b*-value pair (Fig. 2B) showed mostly an ADC increase at the brain parenchyma and the cortical surface. With higher diffusion-weighting ($b=200$ and 1000 s/mm^2, Fig. 2C), both negative and positive changes were observed in the functional ADC map; ADC decreases were detected at the parenchyma as well as at the cortical surface, while ADC increases were seen mostly at the surface of the cortex, where positive change was also observed in both the BOLD map and the functional ADC map of the small *b*-value pair.

To examine whether inflow effects contribute to functional ADC changes observed at the large *b*-value pair, different imaging parameters were used to reduce the inflow effects. As shown in Fig. 2D and E, the spatial extent of positive pixels was significantly reduced (compared with Fig. 2C) when a longer TR of 1 s and a smaller flip angle were used. The average number of positive pixels was 48 ± 18 ($n=6$) and 19 ± 12 ($n=3$) for TR$=0.5$ and 1 s (unpaired *t*-test, $p<0.05$), respectively. In contrast, the number of negative pixels was 83 ± 34 and

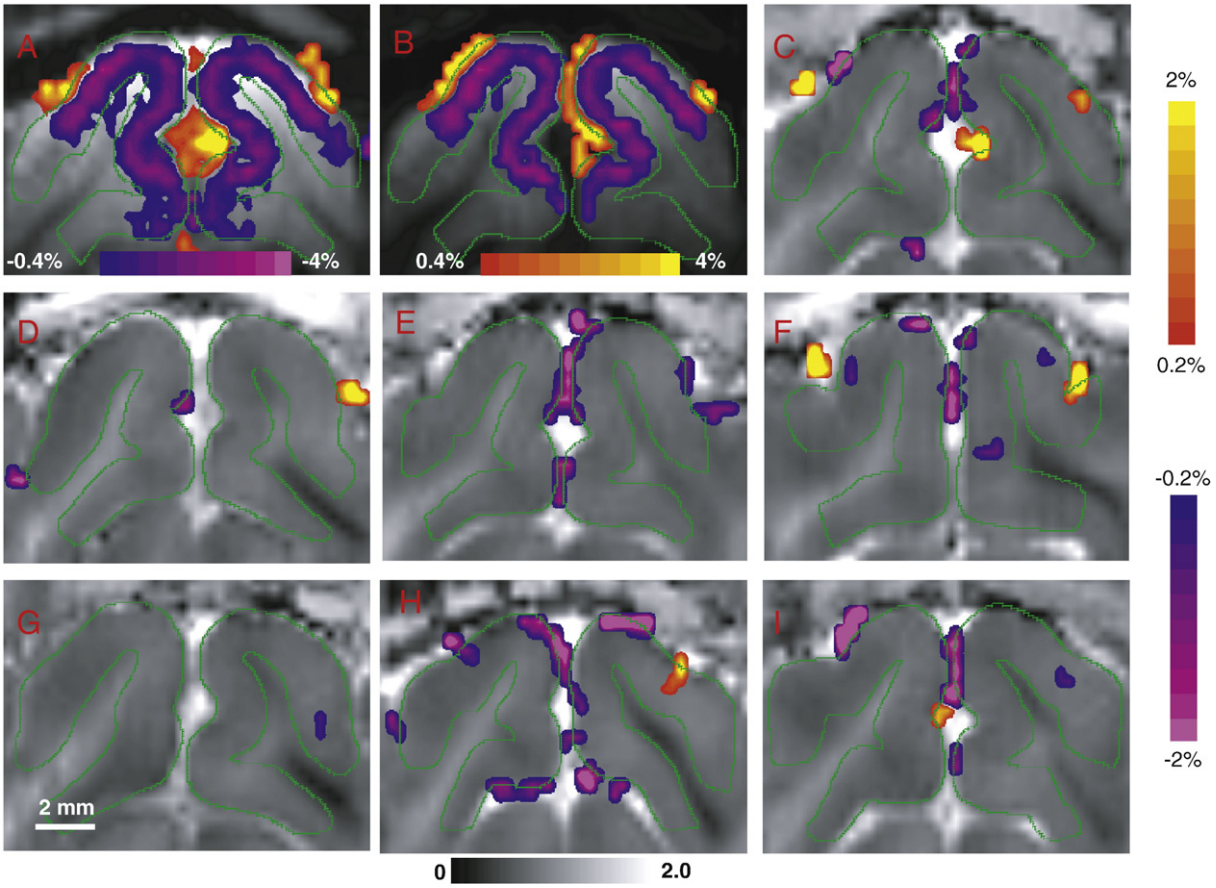

Fig. 4. Functional maps of all seven animals after the removal of intravascular signals with MION. Percentage change maps for DW-fMRI with $b=50$ (A) and $b=1050$ s/mm^2 (B) and the corresponding ADC-fMRI change map (C) were obtained from one representative animal. Gray matter areas were outlined in green. The color bar for DW-fMRI maps is shown in (A) and (B). Horizontal grayscale bars: baseline ADC values in units of 10^{-3} mm^2/s; color bar on right: percentage ADC changes. (D–I) ADC percentage change maps from the other six animals, overlaid on corresponding baseline ADC images. The activated pixels appeared mostly on the cortical surface.

54±7 for TR=0.5 and 1 s ($p>0.1$), respectively. In the middle cortical ROI, the baseline SNR of ADC images was 236±46 and 204±36, and the CNR of $b=200$ s/mm^2 runs was 1.70±0.35 and 1.70±0.18 for TR=0.5 and 1 s, respectively. Because there was no statistically significant difference in SNR ($p>0.3$) and CNR ($p>0.99$), the difference in fMRI maps was not due to the sensitivity, but rather due to the inflow effects.

The averaged time courses with three diffusion-weightings were obtained for the two ROIs illustrated in Fig. 2F, and are plotted in Fig. 3A and B. In both ROIs, all time courses behaved similarly, with higher peak intensities in the surface ROI; functional signal changes (ΔS/S) decreased during the stimulation period, and undershoot after the offset of stimulation. In the middle of the cortex (Fig. 3A), ΔS/S of $b=200$ s/mm^2 was slightly less than that of $b=5$ and 1000 s/mm^2. To examine the dynamics of ADC changes, ADC time courses were determined in the middle cortical ROI (Fig. 3C). Because both negative and positive ADC changes were detected for the large b-value pair at the cortical surface (Fig. 2C), ADC time courses of the surface ROI were not analyzed. The average baseline ADC values ($n=6$) were 0.88±0.06 and 0.72±0.05×10^{-3} mm^2/s in the middle cortical ROI and 1.44±0.11 and 1.04±0.08×10^{-3} mm^2/s in the surface ROI for the small and large b-value pair, respectively. In the middle cortical ROI, ADC responses obtained with the small and large b-value pair showed positive and negative functional changes with ΔADC/ADC of 0.45% and −0.13%, respectively. Unlike DW-fMRI signals (Fig. 3A and B), no significant post-stimulus undershoot was observed in either ADC time course. This can be predicted from similar undershoot magnitudes in DW-fMRI time courses, because the absolute ADC change is proportional to the difference in ΔS/S under the two b-weightings (Jin et al., 2006c).

To compare their temporal characteristics at the middle of the cortex, the averaged ADC responses and the BOLD time course were normalized by their respective peak changes and smoothed by a three-point average (Fig. 3D). It is noteworthy that the comparison of temporal properties of individual animals was not possible due to the low SNR of ADC time courses. Nonetheless, the ADC response from the small b-value pair started to increase earlier but peaked at a later time than BOLD, similar to the time course of the CBV response in tissue from a similar cat visual stimulation experiment (Jin et al., 2006a; Yacoub et al., 2005) (see also Fig. 5A). The ADC response from the large b-value pair rose slightly faster than BOLD for the onset and time-to-peak, and returned to baseline faster after stimulation cessation.

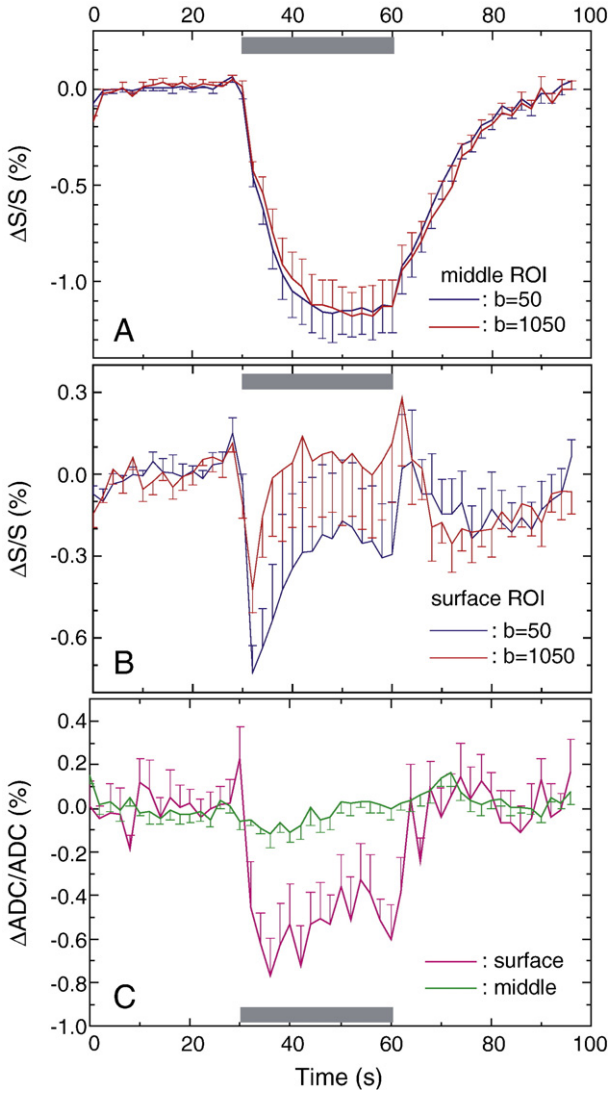

Fig. 5. Average time courses ($n=7$ animals) of fMRI data with MION. (A and B): DW-fMRI data at the middle cortical ROI (A) and surface ROI (B). (C) average ADC time courses ($n=7$) at both ROIs. Decreased ADC changes were detected at the cortical surface, which may have been induced by a partial volume change of CSF. Gray bars: stimulation period; error bars: standard errors of means.

ADC-fMRI with MION: Source of ADC changes

To examine whether the ADC decrease for the large *b*-value pair originated from intravascular sources, blood signals were suppressed by injection of 5 mg/kg MION such that only extravascular signals remained. Figs. 4A and B show DW-fMRI maps for $b=50$ and 1050 s/mm^2 after MION injection, respectively. Note that the MION dose was lower than the dosage used for our CBV-weighted fMRI studies at 9.4 T (≥10 mg/kg) (Zhao et al., 2005). Consequently, for both *b*-weightings, the fMRI signal decreased at the middle of the cortex, while many pixels at the surface of the cortex showed positive changes (see Discussion). The ΔADC/ADC map was calculated from two-*b*-value data; Fig. 4C shows data from the animal in Fig. 4A and B, while Fig. 4D–I show data from the other six animals. Very few activated pixels, either positive or negative, could be found within the parenchyma, while some ADC-decreasing pixels were observed around the cortical surface. The reduction of active pixels after MION injection could partly be due to a lower SNR of the baseline ADC images with MION (156±46, $n=7$) compared with that without MION (225±43, $n=9$) in the middle cortical ROI (unpaired *t*-test, $p<0.003$).

To detect small ADC changes and to compare with ADC dynamics before MION injection (Fig. 3C), time courses were obtained from the middle and surface ROIs (Fig. 5). The time course of $b=50$ s/mm^2 data was very close to that of $b=1050$ s/mm^2 at the middle of the cortex, but was substantially different at the cortical surface ROI. The average baseline ADC value at the middle and surface ROI was 0.74±0.02 and 1.03±0.05×10^{-3} mm^2/s ($n=7$), respectively. The functional ADC change was negligible at the middle of the cortex (−0.03%), but significant (−0.53%) at the cortical surface. Note that the ADC time course in the surface ROI (Fig. 5, magenta) was quite different from the high *b*-value DW-fMRI response (Fig. 5B, red), indicating that their signal sources are different.

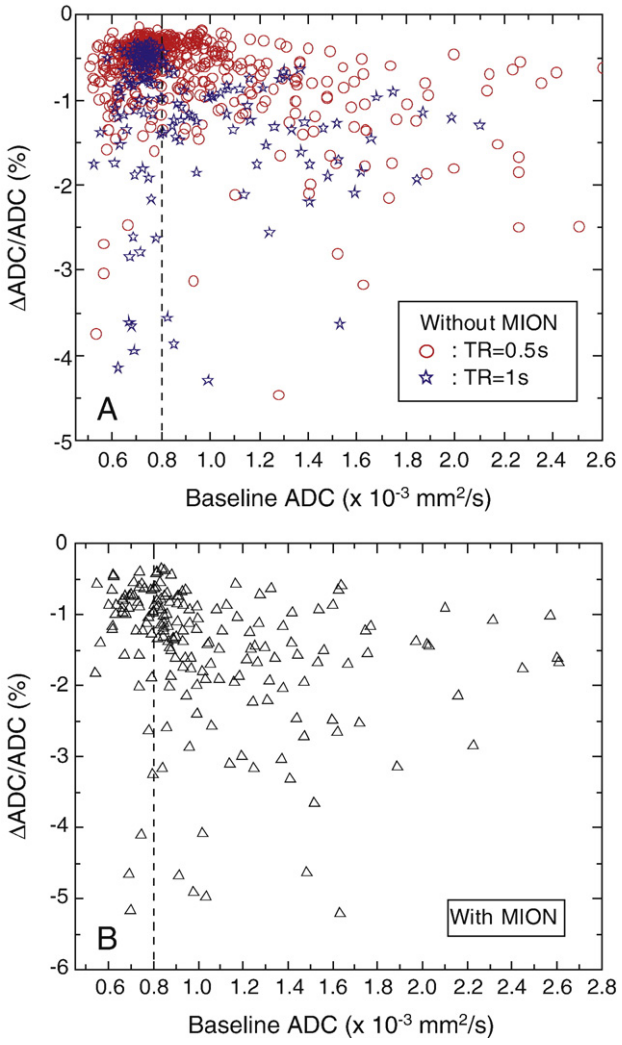

Fig. 6. Sites of functional ADC-decreasing pixels. (A and B): Scatter plot of ADC change versus baseline ADC value for ADC-decreasing pixels without (A) and with (B) MION injection. Without MION, 51.4% and 60% of negative pixels were inside the parenchyma (with baseline ADC ≤ 0.8×10^{-3} mm^2/s, indicated by a vertical dashed line) for TR=0.5 s (n=6) and 1 s (n=3) data, respectively. With MION ($n=7$), 27% of pixels were in the parenchyma.

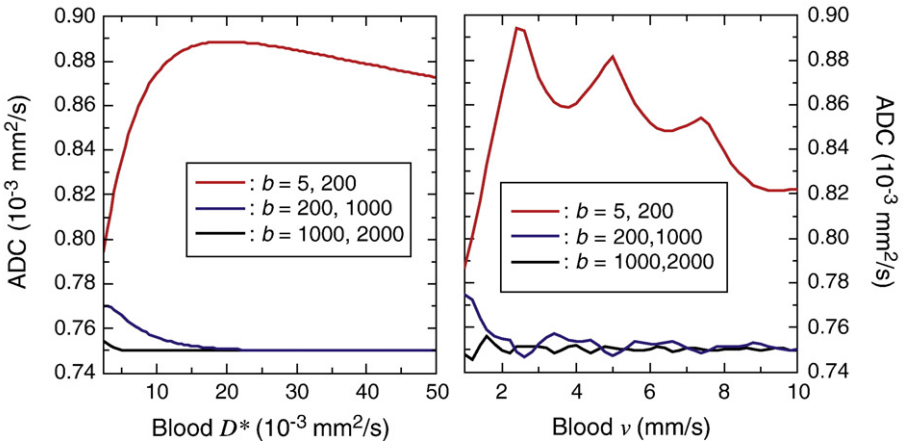

Fig. 7. Simulated ADC values as a function of blood pseudo-diffusion coefficient (A) and blood velocity (B). ADC values were calculated based on Eqs. (2a) and (2b), assuming CBV = 3% and tissue $D = 0.75 \times 10^{-3}$ mm^2/s. Three ADC values were calculated from b-value pairs of 5 and 200 s/mm^2 (red), 200 and 1000 s/mm^2 (blue), and 1000 and 2000 s/mm^2 (black).

Sites of functional ADC decreases

To determine the spatial origin of the negative ADC response quantitatively, baseline ADC versus relative ADC change for ADC-decreasing pixels was plotted in Fig. 6. ADC data without MION obtained from the large b-value pair were used (Fig. 6B)—six animals from TR = 0.5 s (red circles) and three animals from TR = 1.0 s (blue stars) data. Because the pre-stimulus baseline ADC value measured at the middle cortical ROI was $0.72 \pm 0.04 \times 10^{-3}$ mm^2/s without MION (n = 9 animals) and $0.74 \pm 0.02 \times 10^{-3}$ mm^2/s with MION (n = 7), we considered pixels with a baseline ADC $\leq 0.8 \times 10^{-3}$ mm^2/s to be located within the parenchyma, the same cutoff chosen by Song et al. (2002a). Because the ADC of CSF is $\sim 2.5 \times 10^{-3}$ mm^2/s, pixels with significant CSF contribution are expected to have larger ADC values. The fraction of active pixels within the parenchyma was 51.4% and 60% before the MION injection for data with TR = 0.5 s and 1 s (Fig. 6A), respectively, and decreased to 27% after MION injection (Fig. 6B). This indicates that a significant portion of ADC-decreasing pixels were located at the surface of the cortex, especially after the removal of intravascular signals.

Discussion

In our GE-ADC studies of the cat visual cortex, an increase of ADC was observed for a small b-value pair, which can be attributed to blood volume and flow increases. We also found that a decrease in the ADC determined from the large b-value pair within the parenchyma and on the surface of the cortex, but the contrast almost disappeared in the parenchyma and remained at the surface of the cortex after MION injection. A lack of negative ADC change in the parenchyma after the suppression of intravascular signals suggests that the observed negative ADC change is not of tissue origin.

GE-ADC vs. PGSE-ADC measurements

Because the accommodation of diffusion gradients is easier in SE than in GE techniques, most ADC studies with large b-values have used SE approaches. A common diffusion-sensitizing approach is to place two unipolar pulsed-gradients on both sides of the SE refocusing pulse, as proposed by Stejskal and Tanner (1965). As demonstrated in Fig. 1, such PGSE-ADC measurement is affected by the coupling between diffusion and background susceptibility gradients. Because visual stimulation induces a functional ΔR_2 of about -0.2 s^{-1} in cat brain at 9.4 T (Zhao et al., 2004), such blood susceptibility decreases will increase PGSE-based ADC values by 0.2% and GE-ADC values by ~0.03%. In our current GE-ADC experiments with a b-value of 200 and 1000 s/mm^2, ADC decreased about 0.2% (see Fig. 3C), while in our previous PGSE experiments, no detectable ADC change was observed with a b-value of 200 and 800 s/mm^2 (Jin et al., 2006c). This discrepancy can be well explained by the differential coupling effect. Our ADC versus $\Delta R_{2,\ \mathrm{MION}}$ result is consistent with the findings of Does et al., wherein a linear dependence of the PGSE-ADC measurement on the susceptibility effect was observed, and the dependence was stronger for longer TE values (Does et al., 1999). According to a theoretical model (Zhong et al., 1991), the relative change in ADC due to coupling between diffusion and background gradients is proportional to $\Delta \cdot (\mathrm{TE} - \Delta/2)^2$ in a PGSE sequence (Zhong et al., 1991), and is proportional to $\Delta \cdot (\Delta + \delta)^2$ in the GE sequence with bipolar diffusion gradients. Hence, for our parameters in Experiment #1, the contribution of coupling effects to the ADC was proportional to $20 \cdot (45 - 10)^2$ in PGSE versus $9 \cdot (9 + 4.5)^2$ in the GE sequence, which is reasonably consistent with our experimental result, 0.01 versus 0.0012. In order to minimize coupling effects for SE measurements, two pairs of bipolar gradients on both sides of the SE refocusing pulse (Hong and Dixon, 1992), or a double-refocused spin-echo sequence with interleaved bipolar gradients (Le Bihan et al., 2006) can be utilized.

DW-fMRI vs. ADC-fMRI

Although DW-fMRI with a high b-value often indicates the change in water diffusion characteristics during activation (Le Bihan et al., 2006), it should be noted that the signal changes detected by DW-fMRI contain many confounding effects. In DW-fMRI, the signal intensity for GE acquisition can be written as:

$$S(b)/S_0 = \sum_i c_i \cdot V_i \cdot \exp(-b \cdot \mathrm{ADC}_i) \cdot \exp\left(-\mathrm{TE}/T^*_{2,i}\right) \times \left[1 - \exp\left(-\mathrm{TR}/T_{1,i}\right)\right] \quad (1)$$

where i indicates the tissue, arterial and venous blood, and CSF compartments; c and V are the proton density and volume fraction, and T_2* and T_1 are the apparent transverse and the longitudinal

relaxation rates, respectively. Even for a single tissue compartment, it is obvious from Eq. (1) that DW-fMRI signal changes have contributions from the tissue volume fraction change and the change in extravascular T_2* induced by the blood susceptibility effect. The contribution of the susceptibility effect to DW-fMRI is appreciable in Fig. 4B, wherein functional signal decreases at the parenchyma but increases at the cortical surface. Such a spatially opposite contrast is due to the competitive effect of two susceptibility agents: a decrease in deoxyhemoglobin and an increase in MION content. At the middle of the cortex, fMRI signals decreases when the increased field inhomogeneity induced by blood vessel dilation overwhelms the BOLD effect. At the cortical surface with numerous large pial veins, the BOLD effect becomes comparable or larger than the CBV-induced susceptibility change. When blood signal is suppressed using a large *b*-value (at least 1500 s/mm^2) and if the extravascular BOLD signal change is relatively small, decreases in tissue volume fractions may be observable as negative DW-fMRI changes (Harshbarger and Song, 2006).

To obtain information on true tissue diffusivity using fMRI, the aforementioned confounding hemodynamic effects should be minimized. This may be achieved by ADC-fMRI, which is usually calculated from DW-fMRI with two or more different diffusion-weightings (*b*-values). Thus, for the single tissue compartment, the contributions of volume fraction, T_2* and T_1 in Eq. (1), will cancel out, and the change in tissue diffusion can be extracted. In the presence of signals from the blood and CSF compartments, the source of functional ADC change becomes more complicated.

ADC increase in the small b-value regime

In our functional GE-ADC studies with a *b*-value of 5 and 200 s/mm^2, an ADC increase was observed. This is likely caused by an increase in arterial and capillary blood volume and flow (Jin et al., 2006c), because the coupling between background and susceptibility gradients was negligible (Fig. 1) and intravascular venous contribution was minimal due to its short T_2* (shorter than 5 ms at a venous oxygenation level of 60% at 9.4 T (Lee et al., 1999)). The observed ADC increase is consistent with our previous PGSE-ADC data in the same animal model (Jin et al., 2006c). However, compared with the PGSE results, the magnitude of the GE-ADC increase is larger at the cortical surface but smaller at the middle of the cortex. Because the GE-ADC increase at the cortical surface modulates with TR and flip angle, a larger GE-ADC change is mainly due to the inflow effect, which was almost absent in our PGSE results with non-selective excitation. Within the parenchyma, the contribution from the CBV change was expected to be significant (Jin et al., 2006c). This interpretation is supported by the similarity between the temporal characteristics of the ADC and CBV responses: both ADC and CBV changes *at the middle of the cortex* started earlier and peaked later than the corresponding BOLD responses (see Fig. 3D). At *the surface of the cortex*, the onset time and the time-to-peak of CBV were shorter than those of BOLD (unpublished data), suggesting that temporal characteristics are sensitive to the choice of ROI.

Because functional ADC increases in the parenchyma mainly reflect a change in physiological parameters, the quantitative GE- and PGSE-based ADC-fMRI results are expected to be similar at the middle of the cortex. However, the relative ADC change obtained with GE-ADC-fMRI (~0.45%) was only half that of PGSE (Jin et al., 2006c). This discrepancy can be explained by several factors. First, because a functional change of blood susceptibility led to a ~0.2% increase for PGSE-based ADC but not for GE-ADC, the difference in the coupling effect can contribute. Second, a larger initial *b*-value used in our current study (5 s/mm^2 here vs. 2 s/mm^2 in PGSE) led to a greater reduction of signals that originated from fast-flowing blood, decreasing functional ADC change. Finally, GE BOLD signal changes in the current study were about 0.8% in the middle of the cortex, which is less than those in two previous GE BOLD studies (about 1.2% in both) with very similar experimental parameters (Jin et al., 2006b; Zhao et al., 2004), suggesting that different animal groups can contribute to the variation in ADC increases.

ADC decrease in the large b-value regime

Recently, a small functional ADC decrease was observed in humans during neural stimulation with large *b*-values (Darquie et al., 2001; Kershaw et al., 2007; Le Bihan et al., 2006). In *in vitro* and animal studies, large ADC decreases have been reported during intense neuronal activation (Latour et al., 1994; Zhong et al., 1997, 1993), potentially indicating changes in tissue water mobility. On the other hand, Gulani et al. reported that no ADC change was detected for electrical stimulation on excised tissue without any blood, and suggested that the ADC decreases observed *in vivo* might be related to blood flow and volume changes (Gulani et al., 1999). Indeed, our data indicate that activation-induced ADC decreases may not be of tissue origin. When the background susceptibility contribution is minimized using GE-EPI, a weak functional ADC decrease was observed within the brain parenchyma, and responded slightly faster than BOLD at the middle of the cortex. However, the activated pixels within the parenchyma were not well localized to the middle cortical layer, suggesting that the ADC decrease unlikely originated from the tissue diffusion change induced by neuronal activity. Upon the suppression of the intravascular signal using MION, the ADC-decreasing effect at the parenchyma became almost undetectable, indicating that the origin of the ADC decrease observed before MION is likely to be vascular. A vascular source of the ADC decrease is also supported by a recent human hypercapnia stimulation study (Miller et al., 2007). From our data, the underlying physiological sources of functional ADC decreases could be the remaining intravascular signals and partial volume effect of CSF.

Based on computer simulations (see Appendix), slow-moving intravascular signals cannot be fully dephased by a *b*-value of 200 s/mm^2; thus an ADC decrease may arise from an increase in blood velocity in microvessels. In fact, Le Bihan et al. observed a residual vascular BOLD component with a *b*-value of 250 s/mm^2, which was totally removed at higher *b*-values (Le Bihan et al., 2006). Our simulations show that a *b*-value of >1000 s/mm^2 is sufficient to remove all intravascular signals. Therefore, decreases in ADC at very high *b*-values in human studies (e.g., 1200–2400 s/mm^2) can hardly be explained by the remaining intravascular signals. Alternatively, a change in the relative partial volume of fast-diffusing CSF and slow-diffusing tissue components may partially explain ADC decreases at such high *b*-values.

With $b>200$ s/mm^2, ADC decreases were consistently observed at the cortical surface in almost all of our ADC-fMRI studies, namely, using PGSE-EPI (Jin et al., 2006c) and using GE-EPI with and without MION injection. Similarly, large DW-fMRI signal increases in human studies appeared to be close to the cortical surface, even though it was difficult to pinpoint the exact location due to limited resolution (Le Bihan et al., 2006). Nonetheless, the source of these ADC decreases at the cortical surface is certainly not

of neuronal origin. The cortical surface voxels are likely to have a significant partial volume of CSF. Because the water diffusion coefficient in the more compliable CSF compartment is much larger than that in the more rigid tissue compartment, ADC decreases can be induced by a functional decrease in CSF partial volume, which may be caused by either a dilation of the surface vessels or a shift in tissue volume due to parenchymal vessel dilation. Such a hypothesis is supported by a recent report showing a small decrease in CSF partial volume from 10.7% at rest to 10.1% during human visual stimulation, although the variation across subjects was large due to the low sensitivity of the doubling nulling measurement (Donahue et al., 2006). Relative decreases in CSF partial volume of up to ~5% have also been reported during human hypercapania and visual stimulation (Piechnik et al., 2007; Scouten and Constable, 2008). To obtain insight into functional ADC changes, we simulated the ADC using a two-compartment (tissue and CSF) model based on Eq. (1) with tissue D of 0.75×10^{-3} mm^2/s and CSF D of 2.5×10^{-3} mm^2/s, neglecting T_1 and T_2* effects. When the CSF partial volume decreased from 10.7% to 10.1%, the ADC value calculated with our b-values of 50 and 1050 s/mm^2 decreased by ~0.6%, which is fairly consistent with our experimental data (see Fig. 5C). Further experimental and theoretical studies are necessary to examine whether a change in CSF partial volume contributes significantly to ADC-fMRI with higher b-values.

Comparison with human SE ADC-fMRI studies

In DW-fMRI, the extravascular BOLD signal change is usually assumed to be identical for different b-values, and thus is canceled out or minimized in the functional ADC response (Le Bihan et al., 2006). However, this assumption may need further examination. For SE-based fMRI, theoretical models have shown that extravascular ΔR_2 is dependent on vessel size, water diffusion coefficient, and local field inhomogeneity (Boxerman et al., 1995; Fujita, 2001; Kennan et al., 1998; Weisskoff et al., 1994). Consequently, tissue water pools with fast and slow diffusion coefficients may contribute differently to the diffusion-averaging ΔR_2; i.e, $\Delta R_{2,\,slow}\neq\Delta R_{2,\,fast}$. At $b\sim0$, all extravascular water contributes; thus ΔR_2 (and consequently $\Delta S/S$) is a weighted average of $\Delta R_{2,\,slow}$ and $\Delta R_{2,\,fast}$. With a higher b-value, the faster diffusion water pool is suppressed; at an extremely high b-value, only $\Delta R_{2,\,slow}$ contributes to $\Delta S/S$. Such b-value-dependence of $\Delta S/S$ could lead to an apparent change in ADC-fMRI. Recently, Kershaw et al. suggested that signal increases in DW-fMRI with $b>200$ s/mm^2 might be explained by the differential extravascular BOLD effect of fast and slow diffusion components (Kershaw et al., 2007). In our GE-EPI measurements at the static dephasing domain (which is likely to be satisfied at 9.4 T (Yablonskiy and Haacke, 1994)), $\Delta S/S$ is independent of the diffusion effect; thus the contribution of diffusion-dependent ΔR_2 expected in SE acquisitions is likely to be absent. Further theoretical and experimental studies are necessary to evaluate whether the effect of diffusion-weighting on the extravascular T_2 (T_2*) change is significant.

Additional differences between our GE-ADC studies and the human SE ADC-fMRI studies include the ranges of b-values, spatial resolutions, diffusion times, and magnetic fields (Darquie et al., 2001; Kershaw et al., 2007; Le Bihan et al., 2006; Miller et al., 2007). Even at a higher magnetic field of 9.4 T, our small voxel size significantly decreased the SNR compared with low-resolution human studies. In order to achieve an adequate SNR for ADC-fMRI, the b-values used in our study were $\leq$1200 s/mm^2, which is lower than those used in recent human studies (up to 2400 s/mm^2). Although the b-value of ~1200 s/mm^2 is expected to be sensitive to the change of tissue diffusivity with ADC values of $\sim0.8\times10^{-3}$ mm^2/s, a higher b-value could be more sensitive to probe the expansion of a compartment (presumably cell membrane) with a slower diffusion coefficient ($\sim0.2\times10^{-3}$ mm^2/s). In our GE-based ADC-fMRI, the diffusion time was much shorter (5 ms) than that used in human SE-based ADC-fMRI (>20 ms). For restricted diffusion, a shorter diffusion time is less efficient in probing the conformational information of tissue cells and their activation-induced structural changes. The dependence of diffusion time on water diffusivity in brain tissue has been extensively studied; no significant difference in the ADC was detected for t_d longer than 8 ms (Clark et al., 2001; Le Bihan et al., 1993; Moonen et al., 1991; Van Gelderen et al., 1994). Does et al. observed a small increase (~4%) in the ADC in normal rat brain when diffusion time was decreased from 9.75 ms to ~5 ms, and a 24% increase when the t_d value was further shortened to 0.375 ms (Does et al., 2003). These results suggested that a diffusion time of 5 ms could detect conformational changes in brain tissue, similar to longer t_d values, with only slightly lower sensitivity. Although the ADC change of tissue origin could be not observed under our experimental conditions, one cannot rule out the possibility that activation-induced changes in neuronal cell microstructure can slightly affect water diffusivity, which may become detectable with more optimized parameters and improved techniques.

Conclusions

In the small b-value regime (b-value$\leq$200 s/mm^2), functional ADC increases were detected at the parenchyma and at the cortical surface due to blood volume and flow changes. On the contrary, an ADC decrease during brain activation was observed using medium to large b-values ($200\leq b\leq1200$ s/mm^2). However, the spatial pattern of ADC-decreasing responses was not well localized to the middle of the visual cortex. After intravascular signals were totally suppressed using an exogenous contrast agent, ADC decreases were observed mostly at the cortical surface. Thus, an ADC decrease observed at the parenchyma before MION injection has a significant contribution from the residual intravascular signals, and the ADC decrease at the surface of the cortex may be due to a decrease in the partial volume of CSF.

Acknowledgments

This work is supported by NIH grants EB003324, EB003375, and NS44589. The 9.4 T MRI system was funded in part by NIH Grant RR17239. We thank Michelle Tasker and Ping Wang for the animal preparation, Kristy Hendrich for maintaining the 9.4 T system.

Appendix A

The intravascular signal from small blood vessels such as capillaries, small arterioles, and venules may not be fully crushed by medium diffusion-weighting gradients. To examine the contribution from residual intravascular signals, we used a two-compartment model wherein the brain water within the parenchyma consists of tissue and blood. The exchange between blood and tissue compartments is negligible because of the short imaging time (<50 ms) relative to the water exchange time (more than 500 ms) (Labadie et al., 1994; Sanders and Orrison, 1995). According to the IVIM model (Le

Bihan et al., 1986), the attenuation of the blood signal is dependent on the diffusion time of the diffusion gradients, blood velocity, and average length of the vessel segments. If blood water travels through several segments of vessels during the diffusion time t_d, the attenuation of the intravascular signal can be modeled as pseudo-diffusion. Ignoring T_1 and T_2 relaxations, the signal intensity as a function of diffusion-weighting is expressed as

$$S(b)/S_0 = \mathrm{CBV}\cdot\exp\left(-b\cdot D^*\right) + (1-\mathrm{CBV})\cdot\exp(-b\cdot D) = \exp(-b\cdot \mathrm{ADC}) \quad (2a)$$

where CBV is the volume fraction of blood, D^* is the pseudo-diffusion coefficient of the blood, and D is the diffusion coefficient of the tissue water.

If, during the diffusion time, blood water mostly flows within one vessel segment, the blood signal attenuates due to the phase dispersion in the voxel from randomly orientated blood vessels (LeBihan et al., 1988), and the signal intensity can be written as:

$$S(b)/S_0 = [\mathrm{CBV}\cdot|\sin(c\cdot v)/(c\cdot v)| + (1-\mathrm{CBV})]\cdot\exp(-b\cdot D) = \exp(-b\cdot \mathrm{ADC}) \quad (2b)$$

where $c=\gamma\, g\delta\,\Delta$ is the first gradient moment and v the blood velocity. The b-value can be converted to c using $c=\Delta\cdot\sqrt{b/(\Delta-\delta/3)}$. It is assumed that blood water undergoes diffusion in addition to flow, and the diffusion coefficient is assumed to be same as the tissue ADC. In the middle of the cortex, which contains mainly microvessels with an average length microvessel segment l=57 μm and v<5 mm/s (Le Bihan et al., 1988), Eq. (2b) is more relevant to our functional GE experiments with t_d of 5 ms (*i.e.*, during t_d, blood travels a distance<25 μm).

Based on the above equations, ADC values were calculated as a function of D^* or v for three pairs of diffusion-weighting: b=5 and 200 s/mm^2, b=200 and 1000 s/mm^2, and b=1000 and 2000 s/mm^2. We assumed a CBV of 3% and a tissue water D of 0.75×10^{-3} mm^2/s. Fig. 7 shows simulated ADC values as a function of blood D^* or v. The general patterns are similar for both types of signal attenuation. The calculated ADC obtained from small b-values of 5 and 200 s/mm^2 is significantly larger than tissue D. The intravascular signal is mostly crushed for b=1000 and 2000 s/mm^2, wherein the calculated ADC is nearly equal to the tissue D. If the blood velocity in microvessels increases from 1 mm/s to 2 mm/s without any other physiological changes during activation, the ADC value would significantly increase for b=5 and 200 s/mm^2 and would slightly decrease for b=200 and 1000 s/mm^2. Similar results were found for D^*.

References

Boxerman, J.L., Hamberg, L.M., Rosen, B.R., Weisskoff, R.M., 1995. MR contrast due to intravascular magnetic perturbations. Magn. Reson. Med. 34, 555–566.

Clark, C.A., Hedehus, M., Moseley, M.E., 2001. Diffusion time dependence of the apparent diffusion tensor in healthy human brain and white matter disease. Magn. Reson. Med. 45, 1126–1129.

Darquie, A., Poline, J.-B., Poupon, C., Saint-Jalmes, H., Le Bihan, D., 2001. Transient decrease in water diffusion observed in human occipital cortex during visual stimulation. Proc. Natl. Acad. Sci. 98, 9391–9395.

Does, M.D., Zhong, J., Gore, J.C., 1999. In vivo measurement of ADC change due to intravascular susceptibility variation. Magn. Reson. Med. 41, 236–240.

Does, M.D., Parsons, E.C., Gore, J.C., 2003. Oscillating gradient measurements of water diffusion in normal and globally ischemic rat brain. Magn. Reson. Med. 49, 206–215.

Donahue, M.J., Lu, H.Z., Jones, C.K., Edden, R.A.E., Pekar, J.J., van Zijl, P.C.M., 2006. Theoretical and experimental investigation of the VASO contrast mechanism. Magn. Reson. Med. 56, 1261–1273.

Fujita, N., 2001. Extravascular contribution of blood oxygenation level-dependent signal changes: a numerical analysis based on a vascular network model. Magn. Reson. Med. 46, 723–734.

Gangstead, S.L., Song, A.W., 2002. On the timing characteristics of the apparent diffusion coefficient contrast in fMRI. Magn. Reson. Med. 48, 385–388.

Gulani, V., Iwamoto, G.A., Lauterbur, P.C., 1999. Apparant water diffusion measurements in electrically stimulated neural tissue. Magn. Reson. Imaging 41, 241–246.

Harshbarger, T.B., Song, A.W., 2006. Endogenous functional CBV contrast revealed by diffusion weighting. NMR Biomed. 19, 1020–1027.

Hong, X., Dixon, W.T., 1992. Measuring diffusion in inhomogeneous systems in imaging mode using antisymmetric sensitizing gradients. J. Magn. Reson. 99, 561–570.

Jin, T., Kim, S.G., 2007. The apparent diffusion coefficient response during brain activation: a gradient-echo EPI study at 9.4 T. Proc. Intl. Soc. Mag. Reson. Med., Berlin, Germany, p. 23.

Jin, T., Wang, P., Michelle, T., Kim, S.G., 2005. ADC changes during cat visual stimulation measured by gradient-echo and spin-echo at 9.4 T. Proc 13th Annual Meeting, ISMRM, Miami, FL, p. 1489.

Jin, T., Wang, J., Zhao, F., Wang, P., Tasker, M., Kim, S.G., 2006a. Spatiotemporal characteristics of BOLD, CBV and CBF responses in the cat visual cortex. Proc 14th Annual Meeting, ISMRM, Seattle, p. 2762.

Jin, T., Wang, P., Tasker, M., Zhao, F.Q., Kim, S.G., 2006b. Source of nonlinearity in echo-time-dependent BOLD fMRI. Magn. Reson. Med. 55, 1281–1290.

Jin, T., Zhao, F.Q., Kim, S.G., 2006c. Sources of functional apparent diffusion coefficient changes investigated by diffusion-weighted spin-echo fMRI. Magn. Reson. Med. 56, 1283–1292.

Kennan, R.P., Scanley, B.E., Innis, R.B., Gore, J.C., 1998. Physiological basis for BOLD MR signal changes due to neuronal stimulation: separation of blood volume and magnetic susceptibility effects. Magn. Reson. Med. 40, 840–846.

Kershaw, J., Tomiyasu, M., Kashikura, K., Hirano, Y., Nonaka, H., Hirano, M., Ikehira, H., Kanno, I., Obata, T., 2007. An alternative interpretation for stimulus-related signal changes in diffusion-weighted fMRI. Proc. Intl. Soc. Mag. Reson. Med., Berlin, Germany, p. 25.

Kim, S.-G., Hu, X., Adriany, G., Ugurbil, K., 1996. Fast interleaved echo-planar imaging with navigator: high resolution anatomic and functional images at 4 Tesla. Magn Reson Med 35, 895–902.

Labadie, C., Lee, J.H., Vetek, G., Springer Jr., C.S., 1994. Relaxographic imaging. J. Magn. Reson., Ser. B 105, 99–112.

Latour, L.L., Hasegawa, Y., Formato, J.E., Fisher, M., Sotak, C.H., 1994. Spreading waves of decreased diffusion coefficient after cortical stimulation in the rat brain. Magn. Reson. Med. 32, 189–198.

Le Bihan, D., Breton, E., Lallemand, D., Grenier, P., Cabanis, E., Laval-Jeantet, M., 1986. MR imaging of intravoxel incoherent motions: application to diffusion and perfusion in neurologic disorders. Radiology 161, 401–407.

Le Bihan, D., Breton, E., Lallemand, D., Aubin, M.L., Vitnaud, J., Laval-Jeantet, M., 1988. Separation of diffusion and pefusion in intravoxel incoherent motion MR imaging. Radiology 168, 497–505.

Le Bihan, D., Turner, R., Douek, P., 1993. Is water diffusion restricted in human brain white-matter — an Echo-Planar NMR Imaging study. NeuroReport 4, 887–890.

Le Bihan, D., Urayama, S., Aso, T., Hanakawa, T., Fukuyama, H., 2006. Direct and fast detection of neuronal activation in the human brain with diffusion MRI. Proc. Natl. Acad. Sci. U. S. A. 103, 8263–8268.

Lee, S.-P., Silva, A.C., Ugurbil, K., Kim, S.-G., 1999. Diffusion-weighted spin-echo fMRI at 9.4 T: microvascular/tissue contribution to BOLD signal change. Magn. Reson. Med. 42, 919–928.

McCasland, J.S., Woolsey, T.A., 1988. High-resolution 2-Deoxyglucose mapping of functional cortical columns in mouse barrel cortex. J. Comp. Neurol. 278, 555–569.

Miller, K.L., Bulte, D.P., Delvlin, H., Robson, M.D., Wise, R.G., Woolrich, M.W., Jezzard, P., Behrens, T.E., 2007. Evidence for a vascular contribution to diffusion fMRI at high b value. Proc. Nat. Acad. Sci. 104, 20967–20973.

Moonen, C.T., Pekar, J., de Vleeschouwer, M.H., Van Gelderen, P., Van Zijl, P.C.M., DesPres, D., 1991. Restricted and anisotropic displacement of water in healthy cat brain and in stroke studied by NMR diffusion imaging. Magn. Reson. Med. 19, 327–332.

Piechnik, S.K., Evans, J., Bary, L.H., Wise, R.G., Jezzard, P., 2007. Functional changes in CSF volume estimated using spectroscopic water T2 decay measurement. Proc ISMRM, Berlin, Germany, p. 1926.

Sanders, J.A., Orrison, W.W., 1995. Functional magnetic resonance imaging. In: Orrison, W.W., Lewine, J.D., Sanders, J.A., Hartshorne, M.F. (Eds.), Functional Brain Imaging. Mosby, St. Louis.

Scouten, A., Constable, R.T., 2008. VASO-based calculations of CBV change: accounting for the dynamic CSF volume. Magn. Reson. Med. 58, 308–315.

Song, A.W., Fichtenholtz, H., Woldorff, M., 2002a. BOLD signal compartmentalization based on the apparent diffusion coefficient. Magn. Reson. Imaging 20, 521–525.

Song, A.W., Woldorff, M.G., Gangstead, S.L., Mangun, G.R., McGarthy, G., 2002b. Enhanced spatial localization of neuronal activation using simultaneous apparent-diffusion-coefficient and blood-oxygenation functional magnetic resonance imaging. NeuroImage 17, 742–750.

Song, A.W., Harshbarger, T., Li, T.L., Kim, K.-H., Ugurbil, K., Mori, S., Kim, D.-S., 2003. Functional activation using apparent diffusion coefficient-dependent contrast allows better spatial localization to the neuronal activity: evidence using diffusion tensor imaging and fiber tracking. NeuroImage 20, 955–961.

Stejskal, E.O., Tanner, J.E., 1965. Spin diffusion measurements: spin echoes in the presence of a time-dependent field gradient. J. Chem. Phys. 42, 288–292.

Strupp, J.P., 1996. Stimulate: A GUI based fMRI analysis software package. NeuroImage 3, S607.

Tootell, R.B.H., Switkes, E., Silverman, M.S., Hamilton, S.L., 1988. Functional anatomy of Macaque striate cortex. II. Retinotopic organization. J. Neurosci. 8, 1531–1568.

Van Gelderen, P., Devleeschouwer, M.H.M., Despres, D., Pekar, J., Van Zijl, P.C.M., Moonen, C.T.W., 1994. Water diffusion and acute stroke. Magn. Reson. Med. 31, 154–163.

Weisskoff, R.M., Zuo, C.S., Boxerman, J.L., Rosen, B.R., 1994. Microscopic susceptibility variation and transverse relaxation: theory and experiment. Magn. Reson. Med. 31, 601–610.

Windischberger, C., Moser, E., 2000. Spatial resolution in echo planar imaging: shifting the acquisition window in *k*-space. Magn. Reson. Imaging 18, 825–834.

Woolsey, T.A., Rovainen, C.M., Cox, S.B., Henegar, M.H., Liang, G.E., Liu, D., Moskalenko, Y.E., Sui, J., Wei, L., 1996. Neuronal units linked to microvascular modules in cerebral cortex: Response elements for imaging the brain. Cereb. Cortex 6, 647–660.

Yablonskiy, D., Haacke, E., 1994. Theory of NMR signal behavior in magnetically inhomogeneous tissues: the static dephasing regime. Magn. Reson. Med. 32, 749–763.

Yacoub, E., Ugurbil, K., Harel, N., 2005. The spatial dependence of the post-stimulus undershoot as revealed by high resolution BOLD and CBV weighted fMRI. Proc 13th Annual Meeting, ISMRM, Miami, p. 1395.

Zhao, F., Wang, P., Kim, S.-G., 2004. Cortical depth-dependent gradient-echo and spin-echo BOLD fMRI at 9.4 T. Magn. Reson. Med. 51, 518–524.

Zhao, F., Wang, P., Hendrich, K., Kim, S.-G., 2005. Spatial specificity of cerebral blood volume-weighted fMRI responses at columnar resolution. NeuroImage 27, 416–424.

Zhong, J., Kennan, R.P., Gore, J.C., 1991. Effects of susceptibility variations on NMR measurements of diffusion. J. Magn. Reson. 95, 267–280.

Zhong, J., Petroff, O.A.C., Prichard, J., Gore, J.C., 1993. Changes in water diffusion and relaxation properties of rat cerebrum during status epilepticus. Magn. Reson. Med. 30, 241–260.

Zhong, J., Petroff, O.A.C., Pleban, L.A., Gore, J.C., Prichard, J.W., 1997. Reversible, reproducible reduction of brain water apparent diffusion coefficient by cortical electroshocks. Magn. Reson. Med. 37, 1–6.

Zhong, J., Kennan, R.P., Fulbright, R.K., Gore, J.C., 1998. Quantification of intravascular and extravascular contributions to BOLD effects induced by alteration in oxygenation or intravascular contrast agents. Magn. Reson. Med. 40, 526–536.